

DYNAMICS OF SUSPENSION-SLIDER-AIR BEARING SYSTEMS: EXPERIMENTAL STUDY

Q. H. Zeng¹ and D. B. Bogy
Computer Mechanics Laboratory
Department of Mechanical Engineering
University of California
Berkeley, CA 94720

ABSTRACT

The system identification method was applied to measure the dynamic properties of suspension-slider-air bearing systems. The bump responses of the sliders and gimbal structures were measured. The modal parameters, such as frequencies, damping ratios and mode shapes, of the systems were obtained by using the proposed experimental procedure. The dynamic properties of three systems (Types A, B and C) were investigated. It was found that they have quite different properties, and the suspensions (gimbal) significantly affect the dynamic properties of the air bearings. Some gimbal designs generate additional modes in the frequency band of the air-bearing resonance, or introduce additional stiffness and/or inertia constraints to the slider-air bearings.

¹ Visiting researcher, Associate professor, Institute of Vibration Engineering, Nanjing University of Aeronautics & Astronautics, Nanjing, China.

1 Introduction

A better understanding of suspension-slider-air bearing dynamics is important for lower and more stable flying heights, faster slider settling, and more reliable slider-disk interfaces to further improve the performance of hard disk drives. It is essential for the slider's fluctuation induced by the impacts between sliders and disks to be rapidly damped out so that the successive impacts will not drive the slider motion into resonance and result in a crash. Controlling the fluctuation is also important for sliders with MR elements because the fluctuation can thermally induce a MR signal disturbance (Tian, et al., 1997). Therefore, the evaluation of the dynamic properties of the systems becomes an important concern.

Analyzing the dynamic properties requires solving simultaneously the generalized Reynolds equation and the equation of motion of the slider-suspension assembly. Numerical simulation, such as that provided by the CML Dynamic Simulator (Hu and Bogy, 1995), has become a powerful tool for the study of the properties and the design of slider-disk interfaces. The effects of the suspensions can be included in the simulation. However, a reliable and accurate model of the systems is essential for the simulation. The system can be modeled by FE analysis and modal experiment in the lower frequency band in which the properties are mainly controlled by the suspension. The modal superposition method (Cha, 1993) was usually used in the simulation by including the first ten or twenty modes to model the effects of the suspension. In the higher frequency band, the properties are determined by the air bearing. In that range, one often uses three springs and dampers to simulate the effects of the suspension. Because the stiffness of the 50% or 30% slider-air bearings, especially for the sliders with negative pressure, is much larger than the static stiffness of the gimbal, many researchers, such as Hayashi, et al. (1990), Kang, et al. (1995), and Deng, et al. (1997), even ignore the effects of the suspensions in the dynamics of the air bearings. However, recent experiments (Zeng and Bogy, 1997b) show that some gimbal designs also play an important role in the frequency band of the air bearing

resonance. Therefore, it is necessary to investigate the dynamic properties of the system in the higher frequency band to properly model the system.

In this report, the system identification method was applied to measure the dynamic properties of suspension-slider-air bearing systems. The bump responses of the sliders and gimbal structures were recorded. The modal parameters, such as frequencies, damping ratios and mode shapes, of the systems were obtained by using the proposed experimental procedure. Modes in the high frequency band (25-120 kHz) of three systems (Types A, B and C) were measured. It was found that they have quite different properties, and the suspensions (gimbal) significantly affect the dynamic characteristics of the air bearings. The integrated gimbal structures generate additional modes in the frequency band of the air-bearing resonance, or introduce additional stiffness and/or inertia constraints to the slider-air bearings. The preliminary results also show the proposed method is robust for experimentally evaluating the dynamic properties of the suspension-slider-air bearing systems.

2 Experimental Method

2.1 Basic idea and assumptions

This report is a continuation of our previous research (Zeng and Bogy, 1997b). The methods in the previous report will be directly used. Here, we mainly discuss the additional techniques that are used in the current research. Assuming the suspension-slider-air bearing systems are linear, time-invariant, self-adjoint, and with viscous damping, the slider is a rigid body and vibrates in the range near its steady flying state, and the out-of-plane motion of the system can be described by using N ($N \geq 3$) degrees-of-freedom (DOFs), we can identify all dynamic parameters of the system if we can apply artificial excitations to the system and measure both the excitations and the responses of the system. The modal frequencies and damping ratios of linear systems can be identified from free response data even if the excitations are not measured. In this report, we use the

measured free responses of the sliders to bumps on the disks to identify the modal frequencies and damping ratios.

To obtain the mode shapes of the systems, we need more precise control and additional assumptions about the excitations. Because it is difficult to measure the excitations, we attempt to restrict the excitations to an impulse excitation applied at a single point. Assuming the excitations are an impulse applied at the single point, we can use the measured free response data as the impulse response function to estimate the mode shapes. Because the amplitude of the excitation is unknown, the modal masses can not be obtained from the measured data. However, if the system has only three DOFs (three modes) in the frequency band of interest, and the analyzed mass matrix of the slider can be used as the mass matrix of the measured system, the modal masses can be obtained, and thereby the stiffness and damping matrices of the system can also be estimated. It should be mentioned that the assumptions about the excitations only affect the accuracy of the measured mode shapes and matrices, and do not affect the estimation of the frequencies and damping ratios.

2.2 Experimental materials

A 3.5 inch super smooth disk was used in the experiments. The disk was scratched lightly by a sharp knife. For our experiments, the accurate knowledge of the dimensions of the bumps was not necessary. What we required was that the sliders do not severely impact with the bumps, and the bumps could induce sufficiently large fluctuations of the sliders. We used AE signals to monitor the impact between the bump and the sliders.

Three types (Type A, B and C) of the suspension assemblies were used. The air bearing surfaces (ABS) of Type A and B, as shown in Figure 1, are very similar. Both are “advanced air bearing” (AAB) sliders with sub-ambient pressure regions. The load beams of the two suspension assemblies are similar, but their flexures are quite different (see Figure 2 and Figure 5). The flexure of Type A is a two-piece structure. Type B has an

integrated flexure. Type C, shown in Figure 8, has a taper flat slider and a HTI 1650 suspension that has an integrated gimbal.

2.3 Experimental setup

The experimental setup includes a spin-stand, two Laser Doppler Vibrometers (LDVs), a data acquisition system, and computer. We used the Lotus 7000 CSS tester as the spin-stand. It is convenient to use the tester to adjust the rotation speed of the disks, normal loads (or Z-height), and radial position of the sliders. The location of the sliders was set to allow only the outer rail of the sliders to impact with the bump. The relative speed of 14.1 m/s was chosen. The Polytec OSF 1100 LDV was used to measure the velocity responses of the sliders. We used only one beam to measure the absolute responses of the sliders and the gimbals. The fast tracking filter of the LDV was always used to improve the SN ratios because the responses were usually very small. The Polytec OFV 501 LDV was used to measure the bump on the disk. The signal was used to trigger the Data 6000 digital recorder, and to determine the time at which the trailing edge flies over the bump. The Data 6000 digital recorder was used to acquire the responses of the systems. The sample interval was 0.2 μ S, and the number of data points was 2048. Thirty-two records were averaged in the time domain to improve the SN ratios. A band-pass filter with a pass band of 20 kHz to 300 kHz was added between the LDV and the Data 6000. A high pass filter is always necessary for measuring the absolute responses of the systems because the signals of the disk vibration are very strong in the lower frequency band. A program was developed to read the data from the Data 6000 to the PC, and perform the data pre-processing and parameter estimation.

2.4 Experimental procedures

There are two procedures. The first one, which is similar to the procedure described in our previous report (Zeng and Bogy, 1997b), was used to obtain modal frequencies and damping ratios. The procedure is as follows.

1. Create a geometry model of the system to be measured. The model should include several measurement points on the slider and gimbal structure to identify the mode shapes.
2. Measure the bump responses of the slider and gimbal
 - 1) Use one LDV to measure the bump to trigger the DATA6000.
 - 2) Use another LDV to measure the response on a measurement point.
 - 3) Average the measured data in the time domain.
 - 4) Transfer the data to the PC, and save the data and measurement point number.
 - 5) Move the second LDV to a different point, repeat 3) and 4) until all measurement points are measured.
3. Perform the data preprocessing
 - 1) Select the free responses from the bump responses based on the measured bump signal.
 - 2) Perform a time domain filtering to eliminate the noise.
 - 3) Add a non-uniform window to increase the SN ratio.
 - 4) Perform FFTs to obtain the frequency domain data.
4. Estimate the modal frequencies and damping ratios
 - 1) Use time or frequency domain method to estimate the modal frequencies and damping ratios.
 - 2) Remove the effects of the windows on the frequencies and damping ratios.

After the modal frequencies and damping ratios are obtained, the same measured raw data are used to estimate the mode shapes and stiffness and damping matrices. The procedure is as follows.

1. Perform the data preprocessing
 - 1) Recall the measured raw data
 - 2) Select the free responses from the bump responses.
 - 3) Add a non-uniform window to increase the SN ratio.
 - 4) Perform FFTs to obtain the frequency domain data.

2. Estimate the modal shapes

- 1) Use the frequency domain method to estimate the modal frequencies, damping ratios and residues.
- 2) Calculate the mode shapes, by using equation

$$\begin{Bmatrix} \varphi_{1j}\varphi_{lj} \\ \varphi_{2j}\varphi_{lj} \\ \vdots \\ \varphi_{nj}\varphi_{lj} \end{Bmatrix} = \begin{Bmatrix} iA_{1lj} \\ iA_{2lj} \\ \vdots \\ iA_{nlj} \end{Bmatrix} \quad (1)$$

where $i = \sqrt{-1}$, l is the excitation DOF (i.e., trailing edge-outer rail), and A_{nlj} is the residue of mode j at point n . The mode shape φ_{nj} can be found from this equation. The estimated mode shapes are often complex.

- 3) Perform a rigid body motion fit to improve the mode shapes of the slider and obtain the components of the unmeasured points on the slider. Because the slider can be considered as a rigid body in the air bearing frequency band, the mode shape components at the each point should satisfy the following equation

$$\begin{Bmatrix} \varphi_{1j} \\ \varphi_{2j} \\ \vdots \\ \varphi_{nj} \end{Bmatrix} = \begin{bmatrix} 1 & x_1 & y_1 \\ 1 & x_2 & y_2 \\ \vdots & \vdots & \vdots \\ 1 & x_n & y_n \end{bmatrix} \begin{Bmatrix} \varphi_{Zj} \\ \varphi_{Pj} \\ \varphi_{Rj} \end{Bmatrix} \quad (2)$$

where, x_n, y_n are the coordinates of point n with respect to the mass center of the slider. If the number of measured points on the slider is larger than 3, we can use the least square method to find the mode shape components (φ_{Zj} , φ_{Pj} and φ_{Rj}) of the mass center. Then, using Eq.(2), we can obtain the smoothed mode shapes and the components of mode shape of the unmeasured points.

4. Estimate the stiffness and damping matrices. If the system has only three DOFs (three modes) in the air bearing resonance frequency band, we can estimate the stiffness and damping matrices by using the analyzed mass matrix $[Mc]$ and the measured modal parameters. Eq. (2) is used to find the mode shape components of the mass center, and a mode shape matrix is constructed as

$$[\phi] = \begin{bmatrix} \phi_{Z1} & \phi_{Z2} & \phi_{Z3} \\ \phi_{P1} & \phi_{P2} & \phi_{P3} \\ \phi_{R1} & \phi_{R2} & \phi_{R3} \end{bmatrix} \quad (3)$$

and

$$[\Psi] = \begin{bmatrix} [\phi] & [\phi]^* \\ [\phi][\Lambda] & [\phi]^*[\Lambda]^* \end{bmatrix} \quad (4)$$

where

$$[\Lambda] = \begin{bmatrix} s_1 & & \\ & s_2 & \\ & & s_3 \end{bmatrix} \quad (5)$$

$$s_j = -2\pi\xi_j f_j + i2\pi\sqrt{1-\xi_j^2} f_j \quad (6)$$

Then, we can obtain the stiffness and damping matrices by using Eqs. 16-20 in the previous report (Zeng and Bogy, 1997a) .

3 Experimental Results

3.1 Measured data and results for the Type A system

Figure 2 shows the gimbal structure and geometry model of the Type A system. There are seven measurement points on the back of the slider, four points on the gimbal and one point on the dimple. When points 4-7 were measured, the laser beam was focused on the slider through the small holes in the gimbal. Figure 3 a) shows some measurement data in the time domain. This data is obtained by averaging 32 records, and the random noise was removed, so the curves are quite smooth. The trailing edge-outer rail has the largest vibration amplitude, and Figure 3 b) shows that the main component is the roll response. That is because the measurement and excitation are all at the peak of the roll mode shape. If the read/write sensor is mounted on the trailing edge-outer rail, the roll mode will be the most important mode for the stable flying height.

Figure 3 b) shows the frequency domain data measured at three different points. There are three larger peaks in the curves, which should be the three modes of the slider-air

bearing. By the parameter estimation method, we found four modes that are shown in Figure 4. The complete mode shapes are shown in the second column. To clearly exhibit the slider's motion, we show only the slider's mode shapes in the third column. From Figure 4, we can see that the first mode is the gimbal bending mode, and the slider has no obvious motion. The second mode is the first pitch mode of the slider. The modal damping ratio is about 10%. The third mode is the roll mode which has smaller damping. The fourth mode is the second pitch mode. The nodal line of the mode has a small shift and is not parallel to the leading edge.

These experimental results show that we can consider the Type A system as having only three modes in the air bearing frequency band, and thereby describe the system with three DOFs. The gimbal structure doesn't have any obvious effects on the slider-air bearing. We used the slider's dimensions and density to find the analyzed mass matrix, and then calculated the stiffness and damping matrices of the air bearing by using the measured modal parameters. The results are shown in Table 1. The simulation results in which the effects of the suspension are not included are also shown in the table for comparison.

3.2 Measured data and results for the Type B system

Figure 5 shows the gimbal structure and geometry model of the Type B system. There are nine measurement points on the back of the slider, seven points on the gimbal and one point (point 18) on the dimple. When point 8 was measured, the laser beam was focused on the slider through the small slot on the loadbeam. Points 51-53 are on the leading edge, when the vibration was calculated by the rigid body motion fitting.

Figure 6 a) shows some measurement data in the time domain. Comparing Figure 6 a) with Figure 3 a), we can see that the response of the Type B system needs more time to damp out. In particular, the response has a component with a lower frequency and small damping. Figure 6 b) shows the frequency of this component is about 25 kHz. The trailing

edge-outer rail has the largest vibration amplitude, and Figure 6 b) shows that two modes make substantial contributions to the responses. The frequency domain data shown in Figure 6 b) indicate that the Type B system has more than three modes in the air bearing frequency band. By the parameter estimation method, we found seven modes that are shown in Figure 7.

From Figure 7, we can see that the first mode is the gimbal pitch mode whose frequency is about 24 kHz. The figure shows that the slider has a pitch motion with respect to the dimple. Because this mode has low frequency, small damping and a larger component of the shape at the trailing edge, the mode would generate a relatively large fluctuation of the flying height, and thereby affect the drive performance. The second mode is the first pitch mode of the slider, whose damping ratio is much smaller than that of the Type A system. The third mode is the gimbal bending mode coupled with the slider motion. The fourth mode is the slider roll mode, and the fifth mode is the second pitch mode. The sixth mode is the gimbal bending mode coupled with the slider second pitch mode, which has small damping, and affects the air bearing. The last one is the gimbal bending mode, and the slider has no obvious motion in this mode. So this mode has little effect on the air bearing. Totally, the Type B system has at least seven modes in the air bearing frequency band. Most modes are coupled - slider motion coupled with the gimbal deformation. Therefore, the system cannot be modeled as a system with 3 DOFs.

3.3 Measured data and results for the Type C system

Figure 8 shows the gimbal structure and geometry model of the Type C system. Because we could not get a strong enough laser reflection from the back of the slider, all of measurement points are on the gimbal as shown in the figure. The slider is bonded to the central pad, so points 1 to 9 on the pad can be considered as the same points on the slider. Points 10 to 17 are on the gimbal. Point 1 is nearby the center of the trailing edge, and point 2 is near the trailing edge-outer rail. Figure 9 a) shows some measurement data in the time domain. We can see that the responses of the Type C system exhibit a beating

phenomenon, and need much more time for damp out. The trailing edge has a large vibration amplitude, and Figure 9 b) shows that the main components are the responses of two modes with close frequency. The frequency domain data in Figure 9 b) indicate that the Type C system has also more than three modes in the air bearing frequency band. By the parameter estimation, we found seven modes that are shown in Figure 10.

From Figure 10, we can see that the first two modes have a close frequency and similar damping. The first mode is gimbal pitch coupled with slider pitch in phase, and the second mode is gimbal pitch coupled with slider pitch motion out of phase. The second mode can be approximately seen as the 1st pitch mode of the slider. The third mode is the gimbal pitch mode with very small damping. The slider has no obvious motion in this mode, so this mode has little effect on the air bearing. The fourth mode is the slider roll mode. It is interesting to note that this mode has a much smaller response to the bump than was observed in the Type A and B systems. The fifth mode is the gimbal bending mode with very small damping and little effect on the air bearing. The last two modes have close frequencies, small damping, and large contributions to the bump responses. One mode is the slider second pitch mode, another is the gimbal bending mode coupled with the slider roll motion. Thus, the type C system also has at least seven modes in the air bearing frequency band. All of these modes are coupled - slider motion coupled with the gimbal deformation. Therefore, the system cannot be modeled as a system with 3 DOFs.

3.4 Discussions of the experimental results

All of the three systems have three slider modes: the first pitch, second pitch and roll modes. The frequencies of Type C are much smaller than those of Type A and B. That means Type C has much smaller stiffness. That is because the slider of the Type C system is a positive pressure slider. Type A (especially the 1st pitch mode) has larger damping. We think it is the frictional contact between the gimbal and loadbeam that results in the larger damping.

Each of the systems has additional modes. Type A has only one additional mode. It is a gimbal mode. The results show that this mode doesn't significantly affect on the slider's vibration. Type B has at least four additional modes. They are coupled modes of the slider and gimbal. These modes, especially the first additional mode, which has lower frequency and damping, severely affect the dynamics of the slider air bearing. Type C has four additional modes. The seventh mode that is coupled with the slider motion obviously affects the dynamics of the system.

We can not quantitatively estimate the errors of the experimental results, but it is believed that the measured frequencies are very reliable. The damping ratios of some modes, such as mode 3 of the type A, modes 4 and 5 of the Type B, and modes 6 and 7 of the Type C, are also quite reliable for engineering application, while the accuracy of the damping ratios of the other modes would be worse. They may only have qualitative meanings. The measured mode shapes are good enough for identifying the modes.

4 Conclusions

An experimental procedure was proposed to measure the dynamic properties of the suspension-slider-air bearing systems. Three systems have been measured. The results show that:

- 1) The proposed procedure is robust to evaluate the dynamic properties of the suspension-slider-air bearing systems. The accuracy of the modal parameters with lower frequencies would be further improved by dividing the frequency band into two bands in the measurements.
- 2) Different gimbal designs have quite different dynamic properties. Some gimbal structures introduce additional inertia and stiffness constraints to the slider-air bearings. So, the gimbal structure significantly affects the dynamic properties of the slider-air bearings. The effects will be more obvious for smaller sliders.

- 3) The Type A system has much better dynamic properties than Type B and C. The dynamic properties of the air bearing of the Type A system are determined by the ABS of the slider.
- 4) It is necessary to develop an analytical method to model the gimbal structures for the dynamic simulation of the system as Type B or C.

ACKNOWLEDGMENTS

This study is supported by the Computer Mechanics Laboratory at the University of California at Berkeley.

REFERENCES

Cha, E. T., 1993, "Numerical Analysis of Head-Disk Assembly Dynamics for Shaped-Rail Sliders with Sub-ambient Pressure Regions," Ph.D Dissertation, Department of Mechanical Engineering, Univ. of California at Berkeley.

Deng, Z.S., Mitsuya, Y. and Ohka, M., 1997, "Flying Characteristics of Head Sliders When Travelling over Magnetic Disk Surfaces," Proc. Of Intl. Conf. On Micromechatronics for information and Precision Equipment, Tokyo, July, pp. 90-95

Hauashi, T., Fukui, S., Ohhubo, T. and Kaneko, R., 1990, "Dynamic Characteristics of Gas-Lubricated Slider Bearings under High Knuden Number Conditions", J. of Tribology, V.112, pp. 111-118.

Hu, Y. and Bogy, D. B., 1995, "The CML Air Bearing Dynamic Simulator", Technical Report No. 95-011, Computer Mechanics Lab., Dept. of Mechanical Engineering, University of California at Berkeley.

Kang, S. C., Peck, P. R., Jhon, M. S., and Kim, I. E., 1995, "Transient Behavior of Negative Pressure Sliders over Rough Surfaces Including Comparisons with Positive Pressure Sliders", *Proc. Sixth Intl. Symp. Adv. Infr. Storage Proc. system*, ISPS-Vol. 1, pp 7-12.

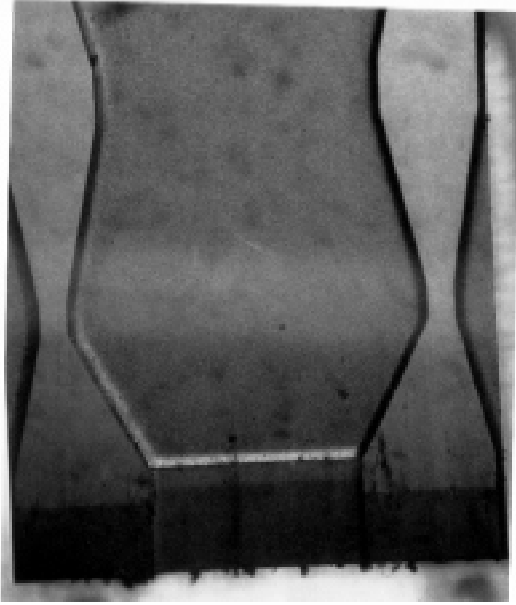
Tian, H., Cheung C.Y. and Wang, P.K., 1997, "Non-Contact Induced Thermal Disturbance of MR Head Signals," *IEEE Tran. on Magnetics*, Vol. 33, No. 5, pp. 3130-3132 .

Zeng, Q. H. and Bogy D. B., 1997a, "Stiffness and Damping Evaluation of Air Bearing Sliders and New Designs with High Damping," Technical Report No. 97-002, Computer Mechanics Lab., Dept. of Mechanical Engineering, University of California at Berkeley (submitted to ASME, Journal of Tribology).

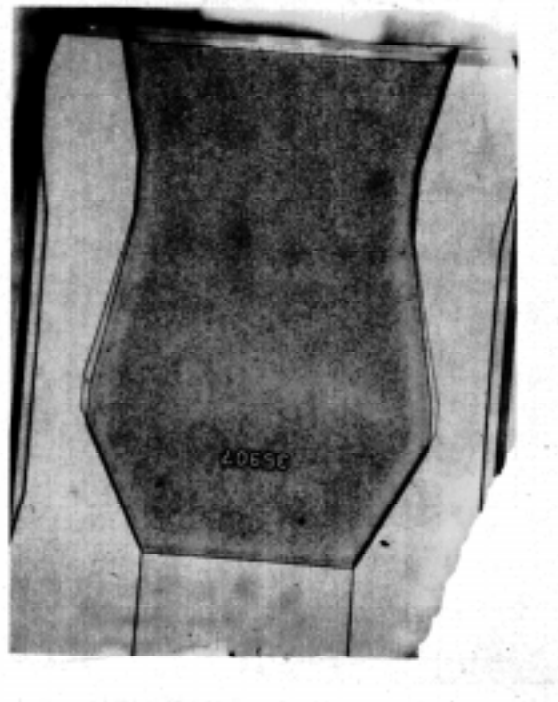
Zeng, Q. H. and Bogy D. B., 1997b, "An Experimental Study on Stiffness and Damping of Air Bearing Sliders," Technical Report No. 97-014, Computer Mechanics Lab., Dept. of Mechanical Engineering, University of California at Berkeley (submitted to ASME, Journal of Tribology).

Matrix	Simulation	Experiment
Stiffness	1.359D+06 -5.796D+02 8.630D-01	1.01D+6 5.13D+2 1.31D+2
	-5.796D+02 6.104D-01 -2.887D-03	5.13D+2 6.06D-1 1.41D-2
	8.630D-01 -2.887D-03 5.711D-01	1.31D+2 1.41D-2 4.40D-1
Damping	7.894D-02 1.182D-05 -1.745D-05	1.76D-1 -8.80D-7 -3.93D-5
	1.182D-05 1.995D-09 2.457D-08	-8.80D-7 1.40D-7 -3.73D-8
	-1.745D-05 2.457D-08 9.485D-08	-3.93D-5 -3.73D-8 7.23D-8

Table 1 Stiffness and damping matrices of the Type A system



a) Type A



a) Type B

Figure 1 Air bearing surfaces(ABS)

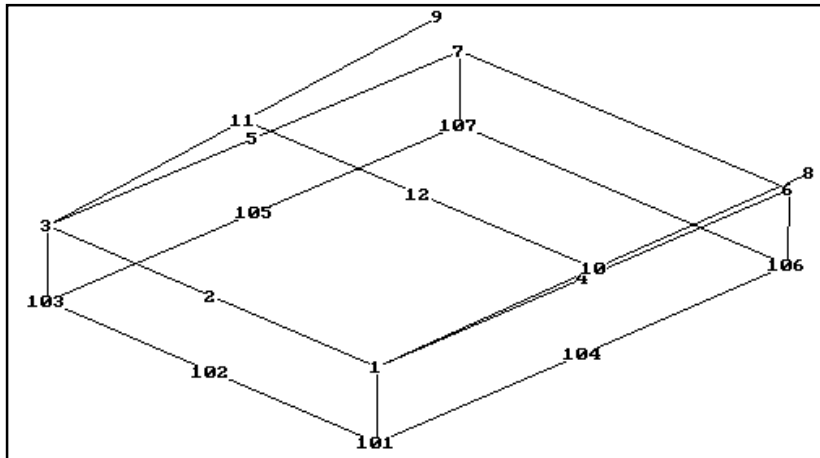
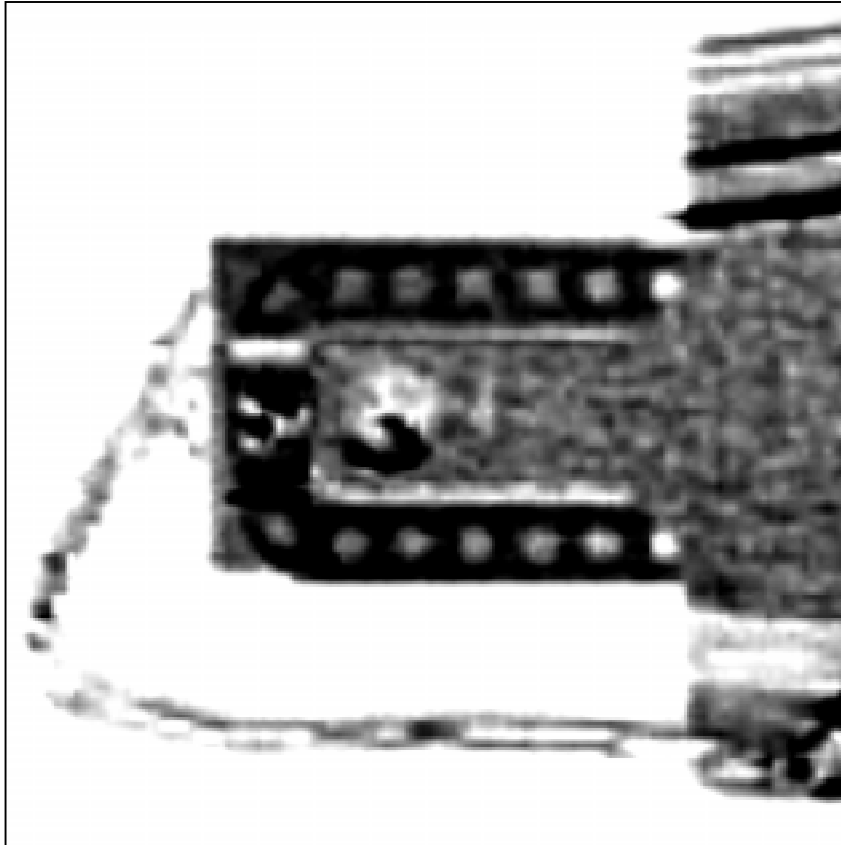


Figure 2 The Type A gimbal structure and geometry model

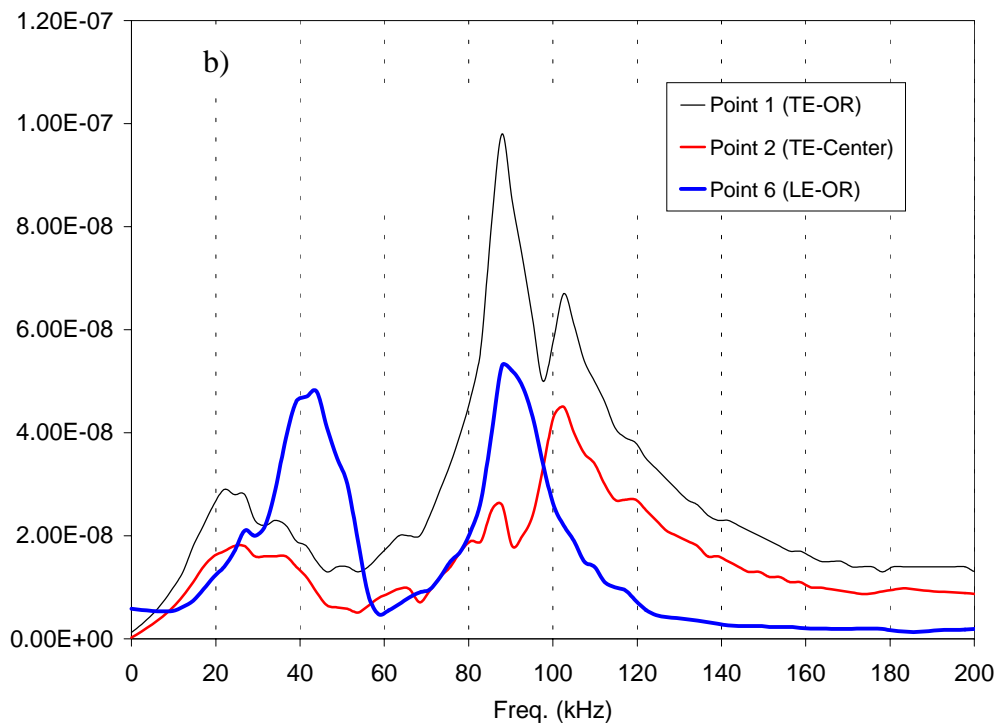
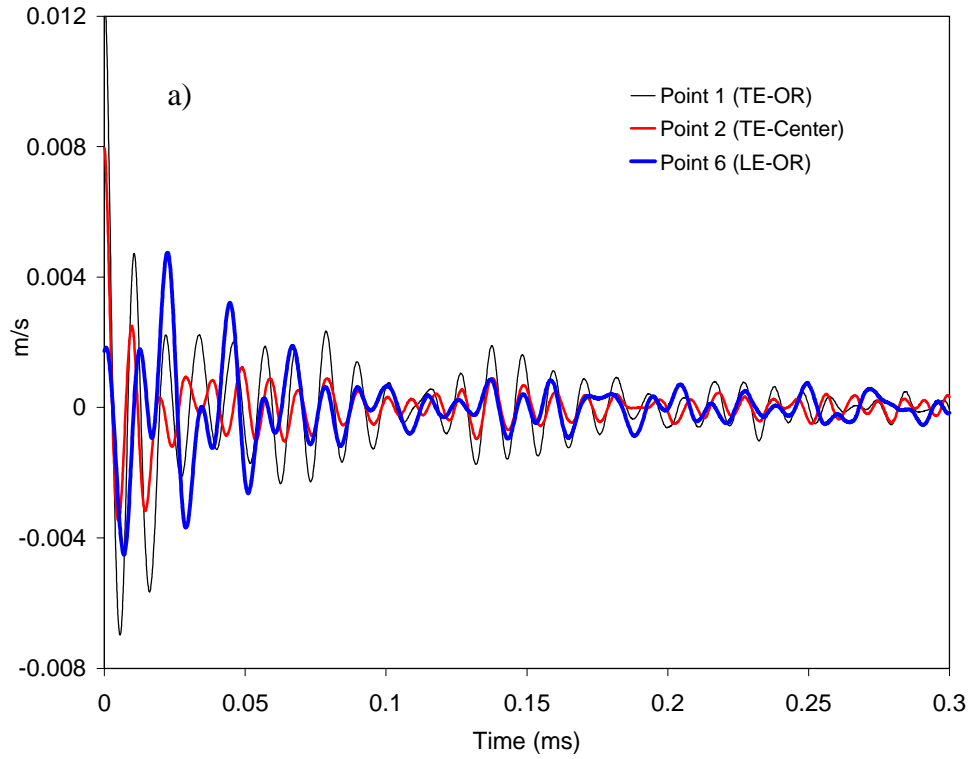


Figure 3 Measured data in the time and frequency domain at the different point of the Type A slider

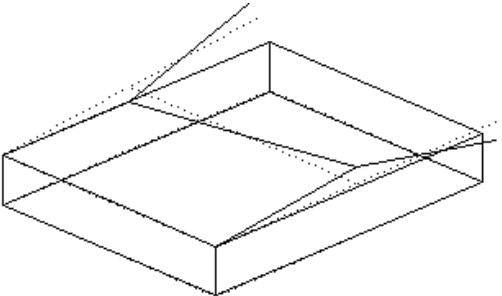
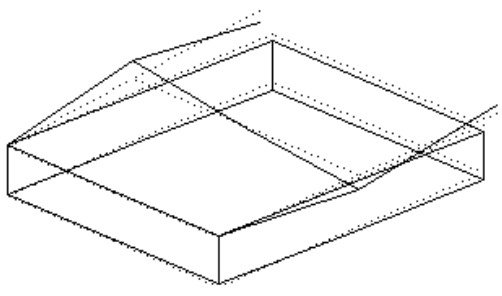
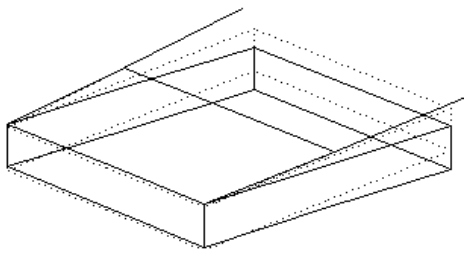
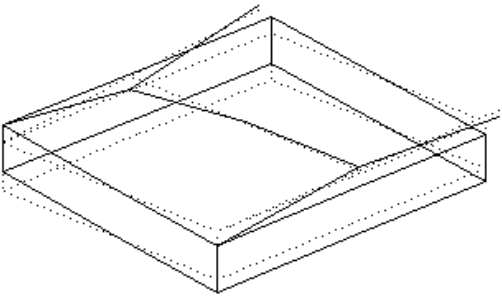
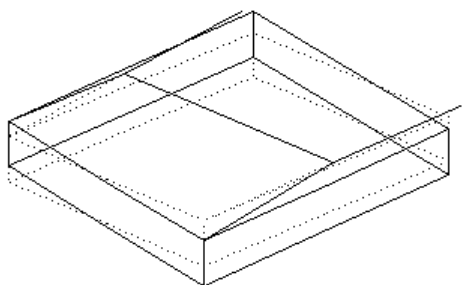
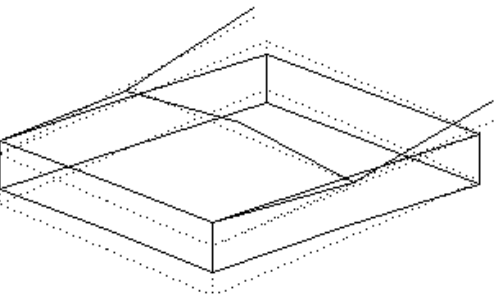
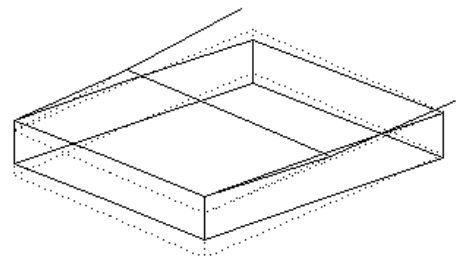
	Show slider and gimbal	Show slider only
1 Gimbal Bending 28.4 kHz 1.33 %		N/A
2 Slider 1 st Pitch 41.1 kHz 10.2 %		
3 Slider Roll 89.0 kHz 3.00 %		
4 Slider 2 nd Pitch 99.8 kHz 2.76 %		

Figure 4 Measured modal parameters of the Type A system

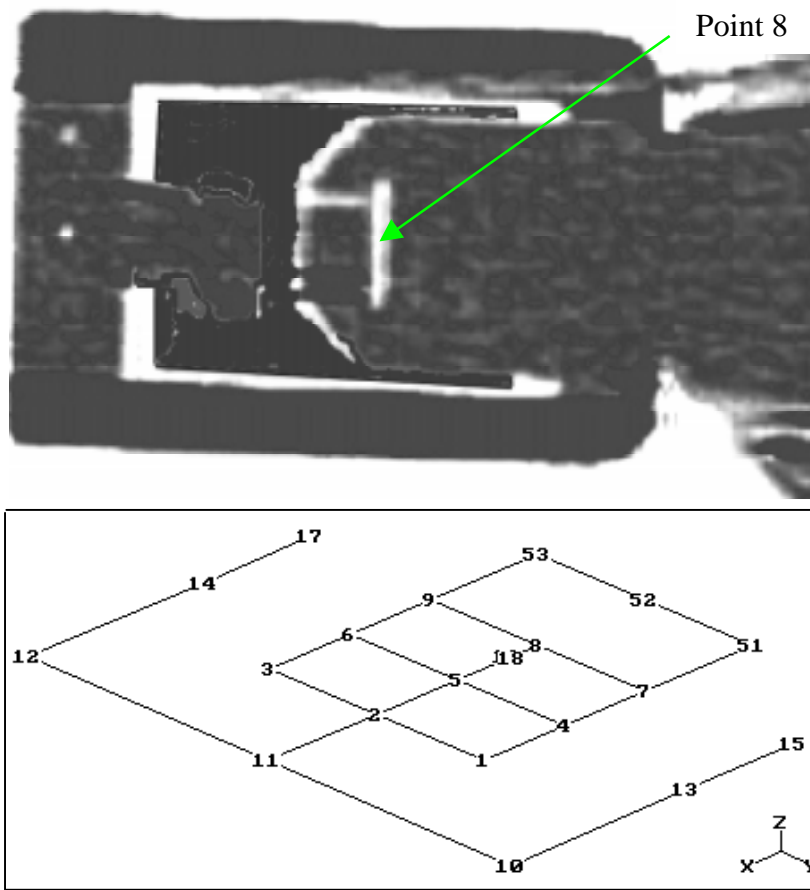


Figure 5 The Type B gimbal structure and geometry model

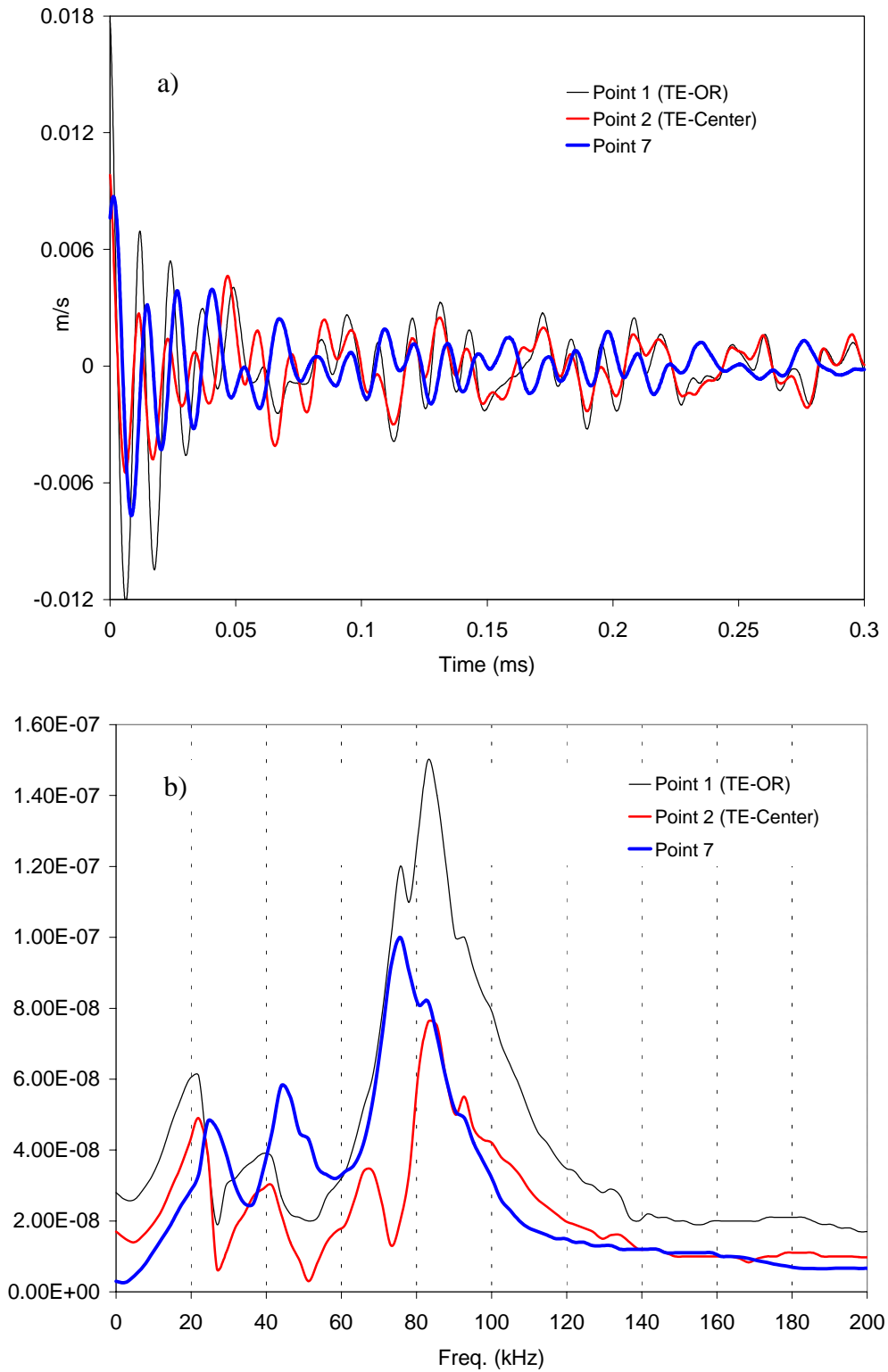


Figure 6 Measured data in the time and frequency domain
At the different point of the Type B slider

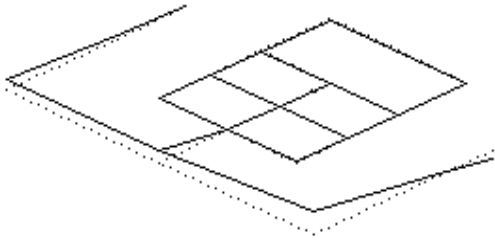
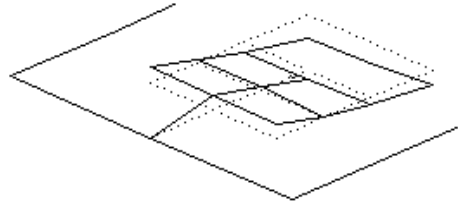
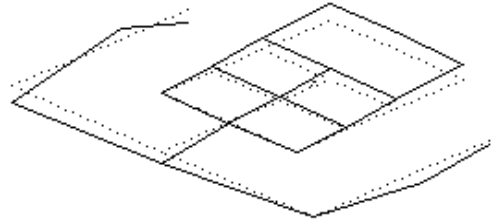
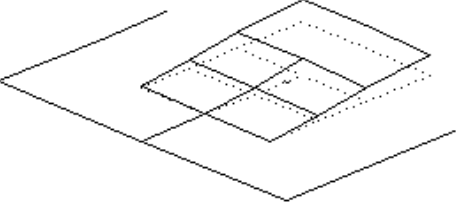
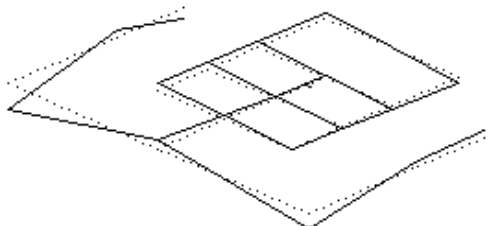
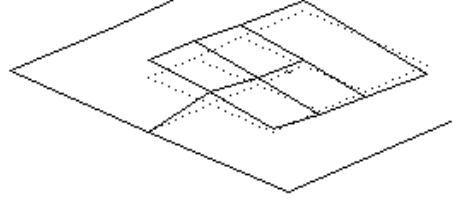
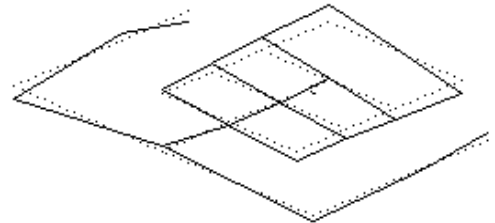
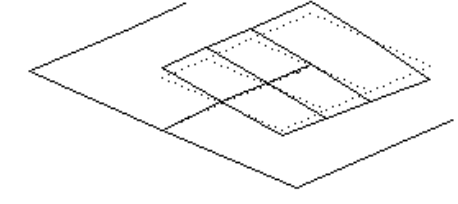
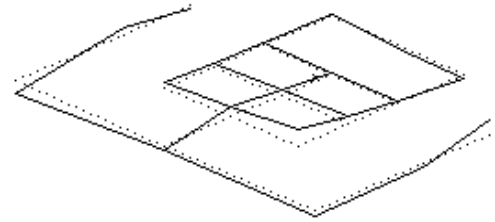
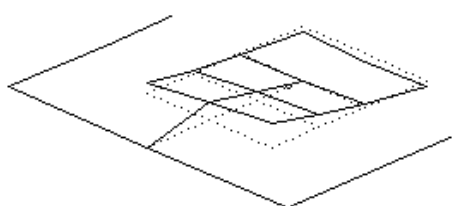
	Show slider and gimbal	Show slider only
1 Gimbal Pitch 24.2 kHz (1.3 %)		
2 Slider 1 st Pitch 44.4 kHz 3.81 %		
3 gimbal bending + Slider Roll 69.0 kHz 3.11 %		
4 Slider Roll 75.2 kHz 3.00 %		
5 Slider 2 nd Pitch 83.4 kHz 2.85 %		

Figure 7 Measured modal parameters of the Type B system

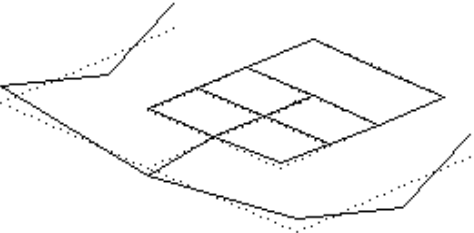
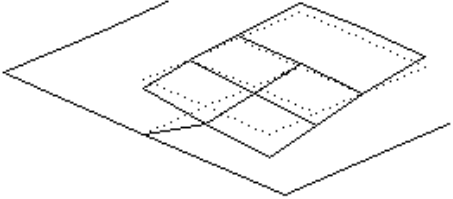
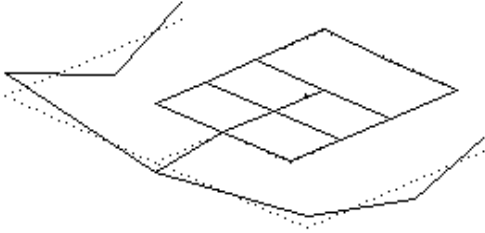
	Show slider and gimbal	Show slider only
<p>6 Gimbal Bending & Slider pitch 91.7 kHz <1 %</p>		
<p>7 Gimbal Bending 96.7 kHz <1 %</p>		<p>N/A</p>

Figure 7 (Continued) Modal parameters of the Type B system

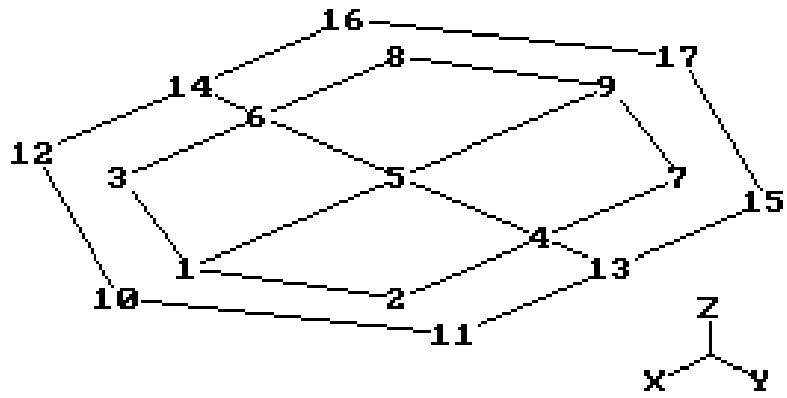
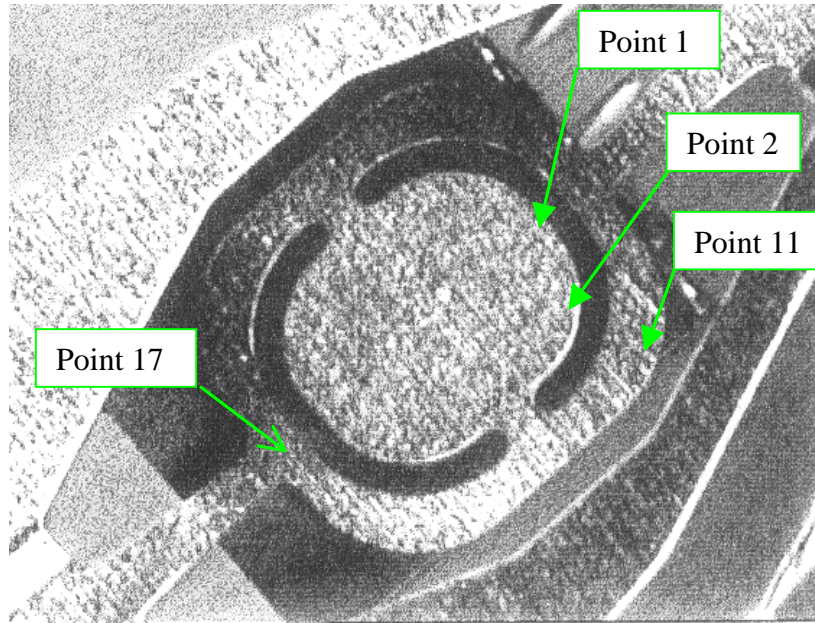


Figure 8 The Type C gimbal structure and geometry model

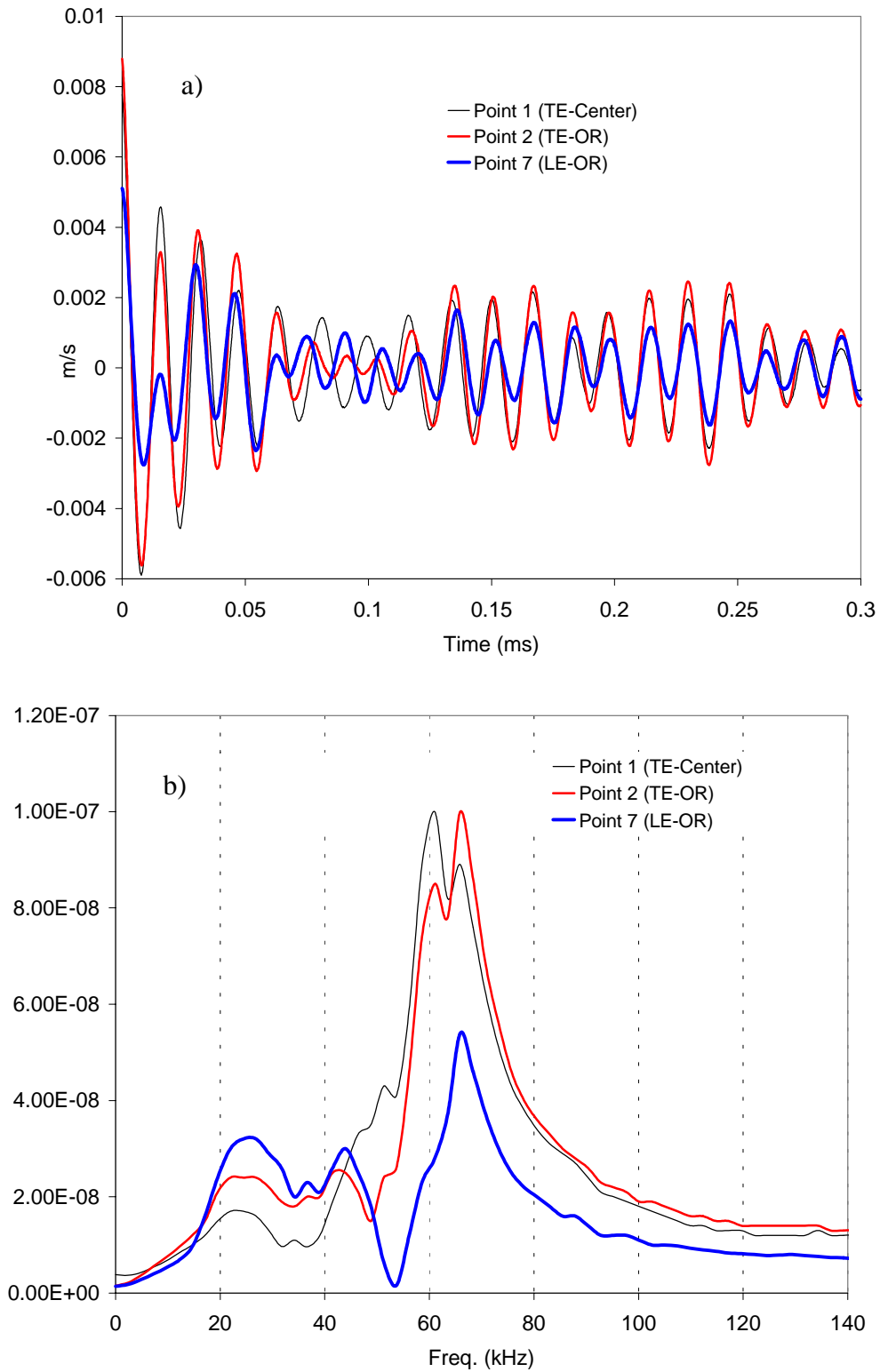


Figure 9 Measured data in the time and frequency domain at the different point of the Type C slider

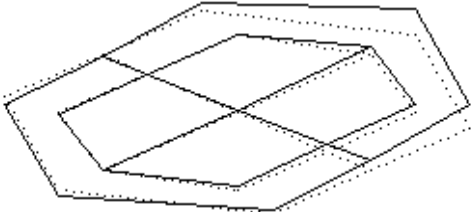
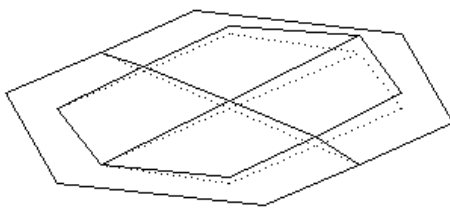
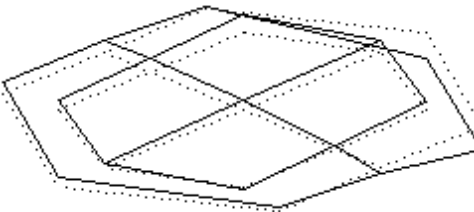
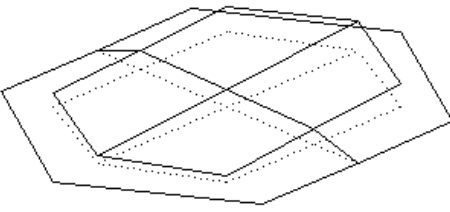
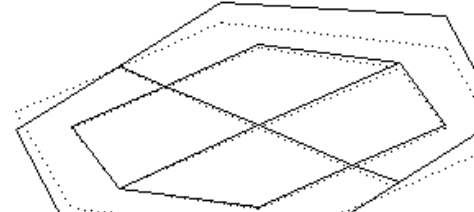
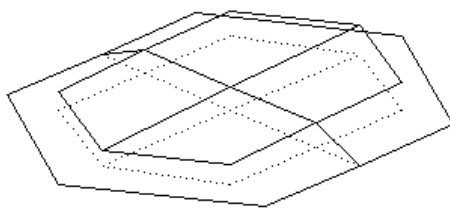
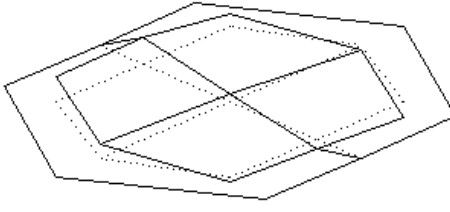
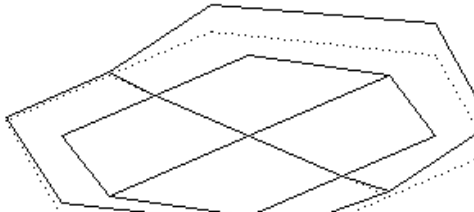
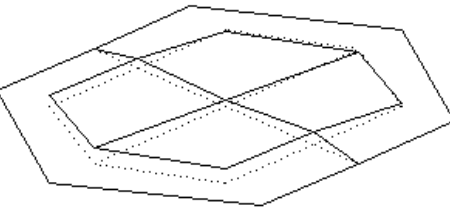
	Show slider and gimbal	Show slider only
1 Gimbal & Slider Pitch 20.6 kHz (7.8 %)		
2 Slider 1 st Pitch 24.0 kHz (8.0 %)		
3 Gimbal Pitch 32.3 kHz 0.93 %		
4 Slider Roll 44.6 kHz 5.63 %	N/A	
5 Gimbal Bending 53.1 kHz <.5 %		

Figure 10 Measured modal parameters of the Type C system

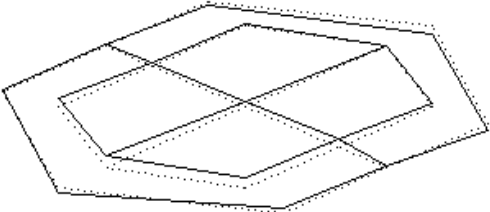
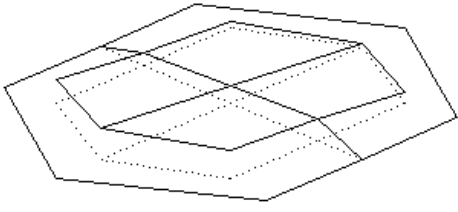
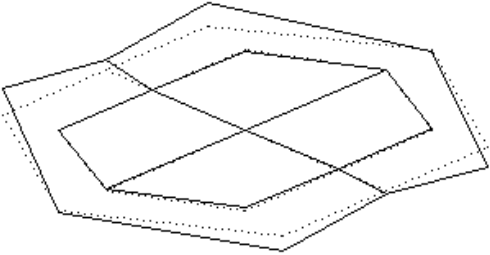
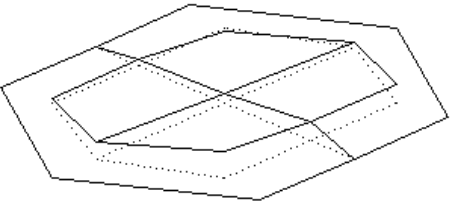
	Show slider and gimbal	Show slider only
6 Slider 2 nd Pitch 60.1 kHz 1.45 %		
7 Gimbal Bending & Slider Roll 64.4 kHz 0.94 %		

Figure 10 (Continued) Modal parameters of the Type C system